Microstructural Heterogeneity for Electrochemical Activity in Polycrystalline Diamond Thin Films Observed by Electrogenerated Chemiluminescence Imaging

K. Honda* and T. Noda

Department of Chemistry and Earth Sciences, Faculty of Science, Yamaguchi University, 1677-1 Yoshida, Yamaguchi-shi, Yamaguchi 753-8512, Japan

M. Yoshimura and K. Nakagawa

Department of Applied Chemistry, School of Engineering, The University of Tokyo, 7-3-1 Hongo, Bunkyo-ku, Tokyo 113-8656, Japan

A. Fujishima

Kanagawa Advanced Science and Technology (KAST), 3-2-1, Sakato, Takastu-ku, Kawasaki-shi, Kanagawa, 213-0012, Japan

Received: May 28, 2004

Electrogenerated chemiluminescence (ECL) was used to image the spatial variations in electrochemical activity at the heavily doped polycrystalline diamond surface. ECL was generated by the reaction of $[Ru(bpy)_3]^{2+}$ and tripropylamine. Images of the chemiluminescence patterns at the polycrystalline diamond surface were recorded photographically after magnification with optical microscopy to show the location and size of individual active regions. The spatial distribution for ECL intensity indicated that the electrochemical reactivity at polycrystalline diamond electrodes was microscopically heterogeneous. The ECL intensities for (100)-oriented growth sectors were much lower than those for other growth sectors, and remained at ca. 50% of those for (111) sectors even at the potential at which the intensity reached maximum. The ratios of the ECL intensities for the (100) sector to the average ECL intensities showed a linear relation with the potential, indicating that the conductivity for (100)-oriented microcrystallite is remarkably lower than that for other types of oriented microcrystallite. Micro-Raman imaging was used to investigate the microcrystallite-based heterogeneity for the conductivity at the heavily boron doped polycrystalline diamond. Raman spectra were collected from an area over $42 \times 42\ \mu m^2$ including (100) and (111) growth sectors at intervals of 3 μm. The map for the intensities of one phonon diamond line reveals that the regions of maximum line intensity correspond to (100)-oriented microcrystallite and the values are approximately 8 times higher than those at (111). The dependence of diamond line intensity on the boron doping levels in diamond indicates that the boron concentration in (100)-oriented microcrystallite is 1 order of magnitude lower than that in (111). Heavily doped polycrystalline diamond film contains microcrystals with different boron doping levels, i.e., semiconductor and semimetallic diamond microcrystals. This microstructural heterogeneity for boron concentration might affect almost all electrochemical activity at heavily doped polycrystalline diamond electrodes.

Introduction

Boron-doped polycrystalline diamond has gained tremendous interest due to its wide electrochemical potential window,[1] small background current in aqueous media,[2] and extreme electrochemical stability.[3] In recent years, numerous studies have been reported on the electroanalytical applications of diamond electrodes as they are thought to be ideal electrode material for electroanalytical detection of biological species.[4−6] As diamond electrode exhibits the low adsorption property for organic compounds, an application study using diamond microelectrodes for in vivo detection of ascorbic acid or glucose in a biological sample (e.g., blood in the human body)[7] has been reported.

However, the diamond electrode does not exhibit electrocatalytic activity, and selectivity for specific compounds is relatively low. For selective detection of biological compounds using a diamond electrode, many studies have employed postcolumn detection with an electrochemical detector.[8,9] Modification of the diamond surface with various catalysts has also been attempted to improve the selectivity of the diamond.[10] However, ideal diamond characteristics, e.g., wide potential window, were partially lost by adding metal catalysts on the diamond surface.

The analytical method using electrogenerated chemiluminescence (ECL) reaction is a promising method to improve the selectivity for amines and oxalic acid without the requirement of pretreatment for the electrode surface.[11] For the ruthenium tris(2,2′)bipyridyl/tripropylamine (TPrA) system, the diamond electrode exhibited a high anodic potential limit (2.5 V vs Ag/AgCl) for the ECL emission due to its wide potential window.[11] The ECL process for $Ru(bpy)_3^{2+}$/TPrA system has two routes

* Corresponding author. Phone: 81 8 3933 5735. Fax: 81 8 933 5273. E-mail: khonda@yamaguchi-u.ac.jp.

10.1021/jp040395z CCC: $27.50
Published on Web 09/16/2004

to generate the oxidized form of TPrA which plays an important role in generating the excited state of $Ru(bpy)_3^{2+}$ *. One route is the homogeneous electron transfer between $Ru(bpy)_3^{3+}$ and amine (catalytic route), and the other route is the direct oxidation of amine at the electrode.[12] At conventional electrodes, e.g., polycrystalline Pt, these routes cannot be separated because the oxidation potentials of $Ru(bpy)_3^{2+}$ and amines are close at these electrodes. However, at the as-deposited diamond electrode, as inner sphere redox species (i.e., TPrA) were relatively oxidized at high overpotential (as in the case of oxygen evolution), clear separation between the catalytic and direct oxidation routes is possible.

The ECL peak potentials for amines through the direct oxidation route showed a close relation to the highest occupied molecular orbital (HOMO) energies, suggesting the possibility for separate detection for various amines by controlling the potential. The diamond electrode exhibited high stability for the $Ru(bpy)_3^{2+}$/amines system;[11] therefore, boron-doped diamond is thought to be a promising candidate for the electrode material for the ECL detector. To develop the ECL detection system with the diamond electrode, it is necessary to optimize the performance at the polycrystalline diamond surface and to achieve a uniformly active surface to detect the co-reactant with high sensitivity.

The objective of this study is to make clear the relationship between microstructure and ECL reactivity at polycrystalline diamond thin films. Several techniques have been developed to image spatial variations in electrochemical activity at the electrode surface. One technique is scanning electrochemical microscopy (SECM), and another method is electrogenerated chemiluminescence (ECL) combined with optical microscopy (ECL imaging). In this study, ECL imaging was used to image spatial variations in electrochemical activity at the polycrystalline diamond surface, particularly to clarify the difference in the reactivity at various types of oriented microcrystallite to optimize the ECL intensity.

The analysis using ECL imaging for the polycrystalline diamond has already been attempted by G. M. Swain et al., and some microscopic heterogeneity for ECL reactivity at the polycrystalline diamond has been obtained.[13] However, the structure−reactivity relationship at the polycrystalline diamond was still not clear. In this study, by selecting the polycrystalline diamond film with nominal crystal size of ca. 5−10 μm, the microcrystallite-based heterogeneity for electrochemical activity could be clearly presented. It has been well-known that, for boron-doped homoepitaxial diamond films and diamond single crystals, incorporation of boron is greater on (111) surfaces than on (100), and the (111) growth sectors contain about 10 times as much as boron as the (100) growth sectors.[14−16] The conductivity of the (111) diamond films is known to be lower than that of films grown on (100) faces. By combining with micro-Raman imaging, we were able to clarify that this difference in the boron doping levels between individual microcrystallites with different growth sectors induced the microstructural heterogeneity for ECL reactivity.

Experimental Section

Highly boron doped diamond thin films were deposited on Si(111) substrates using microwave plasma chemical vapor deposition (CVD) with a commercial microwave plasma reactor (ASTe Corp., Woburn, MA). The details of the deposition process have been described previously.[17] A mixture of acetone and methanol in the ratio of 9/1 (v/v) was used as the carbon source. B_2O_3, the boron source, was dissolved in the acetone−methanol solution at a boron to carbon (B/C) weight ratio of 10^4 ppm. High-purity hydrogen was used as the carrier gas. The bubbling of the acetone−methanol−B_2O_3 solution was carried out at ca. 25 °C. The deposition of the film was carried out at a microwave power of 5 kW. A film thickness of ca. 20 μm was achieved after 10 h of deposition. The typical boron concentration obtained under these conditions is ca. 1.5×10^{21} cm^{-3}.[18] The film resistivity, measured by the four-point probe method, was on the order of 10^{-3} Ω cm.

Micro-Raman scattering experiments were performed on the polycrystalline diamond using a confocal Renishaw micro-Raman system (Renishaw, System 2000) with the 514.5 nm line of an Ar^+ laser as the excitation source. Raman spectra were recorded from the as-deposited diamond top surface with 2−4 μm spatial resolution using a 20× objective to focus and correct the scattered laser light. The laser power at the sample was approximately 3 mW. The spectrometer was calibrated carefully using the silicon Raman mode. Frequency shift resolutions of better than 0.1 cm^{-1} were achieved. The sample was scanned in 3 μm steps underneath the laser beam using a motorized *XY* stage (Renishaw, Model RGH22) over 42×42 μm^{-2} to produce maps of phonon intensity, frequencies, and line widths. Data processing for generating the Raman maps was performed using factory-supplied software (Renishaw, WiRE version 1.3).

In experiments where photographic images of the ECL reactions were recorded, the electrode being studied (polycrystalline diamond) was mounted in an electrochemical cell so that the electrode surface faced upward against an objective lens (20× magnification) and was visualized through a microscope (Olympus, BX51). The electrode surface was covered to a depth of approximately 1 mm with an electrolyte solution containing the compounds required for the ECL reaction. The tip of the KCL agar for the commercial Ag/AgCl reference electrode and a platinum wire counter electrode were immersed in the electrolyte solution. The cell potential was applied with a potentiostat/galvanostat (Hokuto Denko Research, HSV-100). Photographic images were recorded with a CCD camera system (Olympus, DP-70) attached to the microscope. The CCD camera was operated through a personal computer and images were acquired using factory-supplied software (Olympus, DP controller).

All measurements were made at room temperature. Exposure time for the ECL images was typically 5 s. The electrochemical cell was made of Teflon. The working electrode was mounted at the bottom of the cell using a clamp and a Teflon sheet (thickness 0.5 mm). The geometric area of the working electrode was 0.81 cm^2. A block diagram of this setup is shown in Figure 1.

All chemicals were used without further purification. $Ru(bpy)_3Cl_2 \cdot 6H_2O$ (minimum 98%) was obtained from Aldrich (Milwaukee, WI). Tripropylamine (TPrA) was reagent grade quality (Wako, Japan). Tripropylamine was dissolved in 0.2 M phosphate buffer solution (PBS). The pH value of the solution was adjusted to 7.5 with NaOH or NaH_2PO_4. In aqueous $Ru(bpy)_3^{2+}$ ECL analysis, the optimum pH value of the TPrA buffer solution is about 7−8, and the concentrated TPrA (around 100 mM) is usually used to achieve high ECL intensity.[11,12] The solutions were prepared in Milli-Q water (Millipore). The solutions were deoxygenated with nitrogen for 15 min prior to analysis.

Results and Discussion

1. The ECL Image and the Optical Micrograph. Figure 2A shows an optical micrograph of the as-deposited diamond

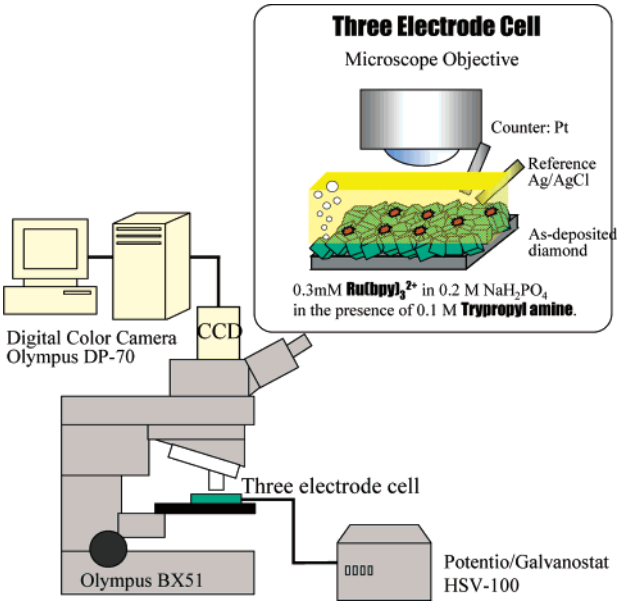

Figure 1. Block diagram of the microscope system capable of observing electrogenerated chemiluminescence.

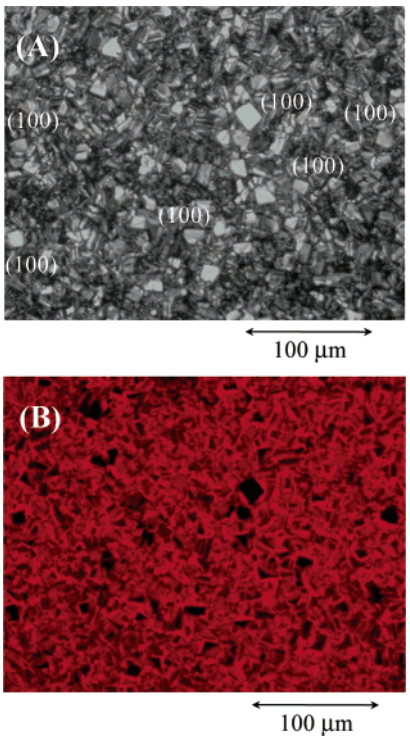

Figure 2. Images of boron-doped polycrystalline diamond surface shown (A) under external illumination and (B) undergoing ECL at 2.0 V vs Ag/AgCl.

surface taken under external illumination at 20×. The polycrystalline diamond is composed of microcrystals with approximately 10 μm grain size. An ECL image at the same region of Figure 2A, taken at an applied potential of 2.0 V vs Ag/AgCl in the presence of the 300 μM $Ru(bpy)_3^{2+}$ and 0.1 M TPrA, is shown in Figure 2B. The ECL image clearly shows the inhomogeneous reactivity for ECL at the polycrystalline diamond surface. Especially at some square-shaped regions, the ECL intensities are remarkably lower than at the surrounding regions. In the optical micrograph, there are a number of square-shaped growth facets (ca. 10 μm grain size). The facet with the well-defined square shape is known to be a (100)-oriented growth facet.[19] By way of comparison of Figure 2A with 2B, the square-shaped dark regions in the ECL image are found to correspond to (100)-oriented growth sectors. It was made clear that the ECL reactivity varies at different types of oriented microcrystallite, resulting in a microcrystal-based heterogeneity for ECL reaction at the polycrystalline diamond.

By use of ECL imaging analysis, the relationship between the electrochemical reactivity and type growth sector of microcrystallite can be clarified. Hence, for microcrystals with outstanding outer shape (e.g., square shape of (100) sector and triangle shape of (111) sector), the potential dependence of the ECL reactivity at the grain surfaces, intercrystalline grain boundaries, and edge regions of microcrystals will be investigated in the following section.

2. Potential Dependence of the ECL Images at the (100) and (111) Growth Sectors. Figure 3 represents the ECL images of the polycrystalline diamond surface at different applied potentials at (A) (100)- and (B) (111)-oriented growth sectors that are observed as square and triangle shapes, respectively. The images were acquired during 5 s chronoamperometric measurements at potentials of (a) 1.2, (b) 2.0, and (c) 2.4 V vs Ag/AgCl.

The average ECL intensities over entire ECL images were calculated using digital image processing software (Adobe, Photoshop 5.0), and the average ECL intensity−voltage profile is shown in Figure 4A. The average ECL intensity started at 1.1 V vs Ag/AgCl, and three ECL waves appeared. The first ECL peak was observed at approximately 1.4 V, followed by a plateau region, and the second peak was obtained at approximately 2.0 V. Beyond 2.0 V, the ECL intensity gradually decreased, and the third ECL wave appeared at approximately 2.3 V as a shoulder. The voltage−ECL curves during cyclic voltammetry (CV) (300 μM $Ru(bpy)_3^{2+}$ in the presence of 0.1 M TPrA) are also shown in Figure 3B. In this measurement, the ECL signal was measured with a photomultiplier (Hamamastu, R928) installed under the electrochemical cell during cyclic voltammograms (sweep rate 50 mV s^{-1}). The ECL behavior during CV (Figure 4B) is quite similar to the behavior of the average intensity at ECL images (Figure 4A). Therefore, the electrochemical reactivity at the polycrystalline diamond characterized using ECL imaging analysis might be reflected in the behavior in the CV.

In ECL images at both growth facets (Figure 3a−c), the average intensity progressively increased with increasing potential up to 2.0 V, and beyond 2.0 V gradually decreased. Even at the lowest potential (1.2 V) for both types of oriented microcrystalline (Figure 3a), the regions with higher ECL intensity could not be observed, suggesting that there is no site with specific activity at the polycrystalline diamond. At a sp^2 carbon electrode such as glassy carbon, it has been reported that the ECL emission started at a lower potential (0.6 V vs Ag/AgCl) than the oxidation potential of $Ru(bpy)_3^{2+}$.[12] In this study, the lowest potential at which ECL images could be clearly observed was approximately 1.1 V. This potential was slightly higher than the start potential of ECL emission in the CV (1.0 V). This difference might be due to low sensitivity of the CCD camera used for the image capture. To clarify the existence of the specific active site (i.e., sp^2 carbon inclusion at the polycrystalline diamond), highly sensitive ECL imaging analysis will be carried out.

For the quantitative comparison of the ECL reactivity at various types of oriented microcrystallite, the ECL intensity−voltage profiles were constructed for (100)- and (111)-oriented growth sectors. The points examined here were selected at the

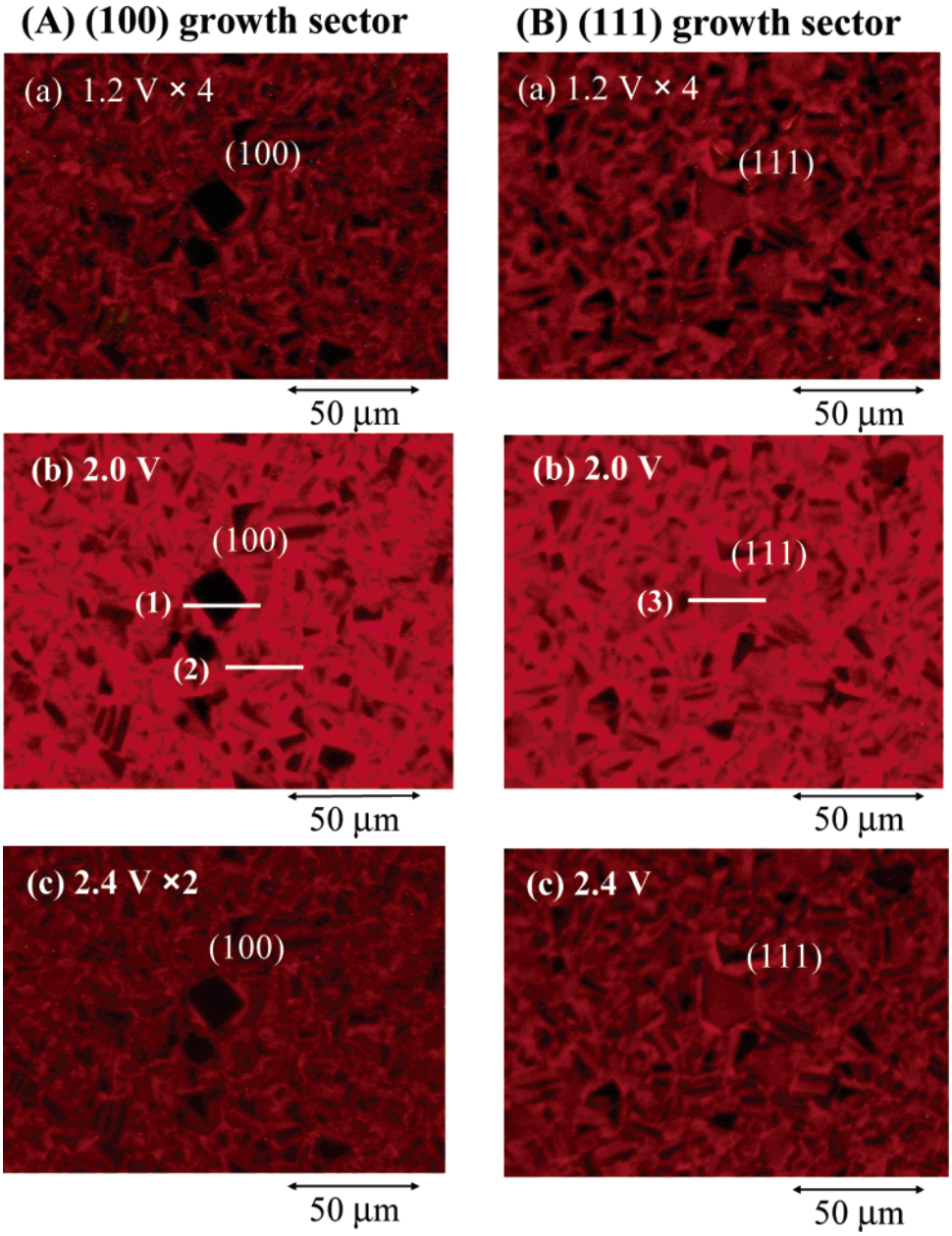

Figure 3. Images of the boron-doped polycrystalline diamond electrode during chronoamperometric measurements of the electrogenerated chemiluminescene reaction at (a) 1.2, (b) 2.0, and (c) 2.4 V in 0.2 M phosphate buffer solution containing 300 μM $Ru(bpy)_3^{2+}$ and 0.1 M TprA. Images were corrected for polycrystalline films centered at (A) (100) and (B) (111) growth sectors. The initial potential was 0.4 V, and the step duration and image collection time was 5 s. "×4", e.g., refers to the number of magnification (4 times) of the light intensity.

center points of (100) and (111) growth facets and a randomly selected region, shown as lines in Figure 3. In the ECL intensity−voltage profile (Figure 4A), the intensity at the (100) facet range is 0.2−0.5 of the corresponding average ECL intensity in the potential regions from 1.1 to 2.5 V, indicating that the ECL reactivities at (100) are approximately 0.2−0.5 of the average. In contrast, the ECL intensities for the (111) facet are equal to those at the surrounding regions, as shown in Figure 3B. The ECL intensity−voltage behavior (Figure 4) is also similar to the average ECL intensity. The intensities for the (111) facet are approximately 1.2 times higher than the average values over the potential range examined, indicating that the reactivity at the (111) facet is slightly higher than the average. Supposing that the polycrystalline diamond is composed of two types of oriented microcrystallite ((100) and (111)), the ratio of the number of (111)-oriented microcrystallites to the total number of microcrystallites could be estimated to be 0.92 using the intensity ratios for the (100) and (111) facets in the potential range from 1.8 to 2.2 V.

In Figure 3A-b, the regions that exhibit the highest ECL intensity correspond to the edges on the (100) growth sectors. On the (100) growth sector, the concentration of the reactant molecules was relatively higher due to the lower ECL reactivity. At the edges of (100), the reactant molecules might be supplied from the electrolyte phase adjacent to the (100) facet by parallel diffusion to the electrode surface, as well as planar diffusion perpendicular to the surface. Therefore, the reactivity at the edges on (100) might exhibit the highest intensity due to the increase in the amount of the reactant.

3. Line Plot Analysis for the ECL Images. For the polycrystalline diamond, some of the grain boundaries have been clarified to incorporate amorphous carbon or specific defects using Raman spectroscopy,[20] and the intercrystalline grain boundaries have been reported to be the active regions for the

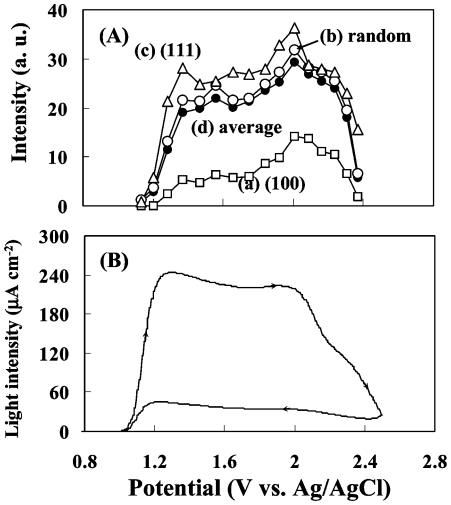

Figure 4. (A) Relationship of electrogenerated chemiluminescence intensity and applied potential obtained from ECL images (Figure 3). ECL intensity was presented at (a) (100) and (c) (111) facets, (b) randomly corrected position, and (d) average values for all over the image. (B) Voltage ECL curves at the as-deposited diamond electrode during a potential scan. Sweep rate 50 mV s^{-1}. Solution condition was the same as (A).

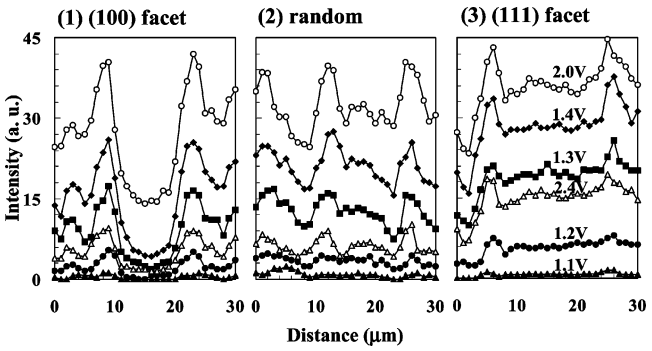

Figure 5. ECL intensity as a function of applied potential for three selected regions of the boron-doped polycrystalline diamond surface. The three selected regions are presented in Figure 3 as horizontal bars.

electrochemical reaction in the luminol/H_2O_2 system.[13] To obtain detailed information on the structure−reactivity relationship (e.g., types of growth sector, grain boundaries) at the polycrystalline diamond, the variations in the ECL intensities on the lines including (100) and (111) growth sectors and intercrystalline grain boundaries (line plot analysis) were examined. Figure 5 shows the potential dependence of the line profiles of the ECL intensities at three selected regions. The three specific regions are indicated by white lines in Figure 3: (1) the line across the (100) growth sector (Figure 3A-b); (2) the line on the region randomly selected (Figure 3A-b); (3) the line across the (111) sector (Figure 3B-b). The linear distance across each profiled region is approximately 30 μm.

In Figure 5-1, for the region across the (100) growth sector, the ECL intensity clearly increased with increasing potential up to 2.0 V while keeping the feature of the profile. Beyond 2.0 V, the ECL intensity gradually decreased and reached the anodic limit for the ECL emission at 2.5 V. The active sites represented by the ECL peaks (8 and 23 mm positions) were positioned at the same regions and are independent of the potential. The appearance of new active sites at higher potential could not be observed.

The intensities at the surface of (100)-oriented microcrystallite (the region between 12 and 20 μm in profile 1) show the lowest level of the ECL intensity, and even at the potential at which

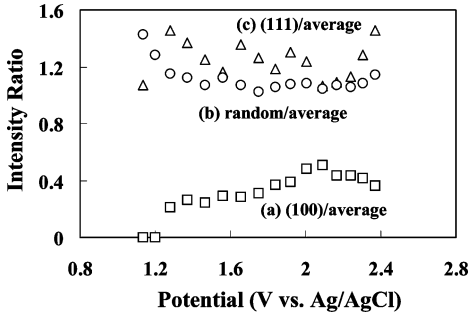

Figure 6. Relationship of ECL intensity ratio of (a) (100) and (c) (111) growth sectors and (b) randomly selected region to applied potentials. ECL intensity ratio is defined as the ratio of the ECL intensity at each growth facet to the average ECL intensity over the surface.

the average ECL intensity reached the maximum (2.0 V), the intensities for (100) remain at approximately 50% of those for (111), indicating that the ECL reaction rate on the (100) surface is approximately 50% of (111) (the region between 9 and 24 μm in profile 3) at a maximum.

Figure 5-1 shows that two sites at the 8 and 23 μm positions of the line profile that correspond to the edges of the (100) facet are the most active for ECL, as evidenced by the highest peaks. The values of the peak width are about 5 μm, and the intensities of both peaks are 1.3−1.4 times higher than those at the outer sides of these peaks.

In Figure 5-3, two peaks are observed at the ridges on the (111) growth sector at the 6 and 26 μm positions. The peak values are approximately 1.2 the intensities on the surface of the (111) growth sector. In addition, in Figure 5-2, three active regions that correspond to the grain ridges and the intercrystalline grain boundaries (2, 12, and 26 μm positions) are observed. The intensities of these peaks are at the same level as the peaks at ridges of (111). For both regions, the ECL intensities increased with increasing potential while keeping the feature of the line profiles, indicating the independence of the position of the active sites on the potentials. At these positions, the ECL started from the oxidation potential for $Ru(bpy)_3^{2+}$ (ca. 1.0 V vs Ag/AgCl), suggesting that the higher reactivity might not be related to the nondiamond carbon impurities.[12] Hence, a possible explanation for the higher reactivity at these ridges is the effect of the three-dimensional structure of microcrystallite. Recent work with the electrochemical behavior of the ECL reaction of $[Ru(bpy)_3]^{2+}$ and tripropylamine using ac impedance measurement has shown that this ECL reaction at the as-deposited diamond electrode has mass transport controlled kinetics in the potential region from 1.2 to 2.0 V.[11] As the ridges of microcrystallite form the pointed-edge lines toward the electrolyte, the reactant molecules could be supplied to the ridge regions by semispherical diffusion, and the reaction rate for ECL was thought to be slightly enhanced by the effect similar to that of a microelectrode.

At the ridge regions on the (100) growth sector (Figure 5-1), the intensities of the peaks were highly enhanced (ca. 1.3−1.4) even at the lower potential (1.3 V vs Ag/AgCl). The strong enhancement at the ridge regions on the (100) sector might be due to the combination of the microelectrode effect at the ridges and the increase in the amount of the reactant molecules supplied from the electrolyte phase on the (100) facet by parallel diffusion.

To illustrate better the effect of the type of growth sector for ECL reactivity examined here, the ECL intensity ratios were used (Figure 6). These values (R) are the ratios of the intensities at each growth sector to the average ECL intensities. The

positions examined for R were the middle points of the lines presented in Figure 3. In Figure 6, the ratios for the (111) sector and randomly selected region are independent of the potential and are constant values (approximately 1). In contrast, for the (100)-oriented growth sector, the ratios depend linearly on the potential. These results indicate that the (100) growth sector required more overpotential than other regions to drive the ECL reaction. This requirement of overpotential is thought to be simply due to the lower conductivity at the (100)-oriented growth sector. Therefore, it can be supposed that the microcrystallite-based heterogeneity for the ECL reaction is related to the difference in the conductivity from growth sector to growth sector. To clarify this supposition, the distribution of the conductivity on the polycrystalline diamond surface will be examined in the next section.

4. Raman Imaging. Recent work on the relationship between Raman spectra and the boron doping level for the diamond microcrystals has shown that the diamond Raman line becomes asymmetrical and its intensity decreases rapidly with increasing doping level above 2×10^{-19} cm^{-3}.[19] Boron works as an impurity, and its doping level in the diamond controls the conductivity of the films. Assuming an inverse linear relation between the intensity of the diamond Raman line and boron concentration in microcrystallites at the polycrystalline diamond,[19,21] the difference in the boron concentration (conductivity) between individual microcrystals was examined using Raman spectroscopic mapping.

An optical image of the polycrystalline diamond surface is presented in Figure 7A. In the center of Figure 7A, there is a 42×42 μm^2 region, represented as the highlighted box, that indicates where the Raman spectra were acquired. The (100)-oriented growth sector that has the square shape and the (111) facet that has the triangle shape can be identified in Figure 7A. Raman spectra were acquired at 3 μm intervals (12 spectra per line and 12 lines) using an acquisition time of 5 s per spectra. The spectral maps constructed from the map of the line intensity, the line position, and the full width at half-maximum of one phonon diamond line are presented in Figure 7B−D. The line intensity, the line position, and the line width were obtained by fitting all spectra with the Lorentzian line shape.

The intensity of the diamond Raman line varies widely over the polycrystalline diamond surface (Figure 7B), which indicates that the boron doping level is not homogeneous across the sample. The regions of maximum intensity (about 4000 counts s^{-1}) correspond to the regions around the (100) growth sector (Figure 7A). In contrast, the values around the (111) sector are about 500 counts s^{-1} and are a factor of 8 less than that for (100), suggesting that the boron doping level at the (100) growth sector is significantly (about 8 times) less than that of the (111) sector. The precise value of the difference in the boron concentration at (100) and (111) growth sectors will be discussed in the following section.

The line position varies from 1310 to 1331 cm^{-1} over the surface of the film (Figure 7C). The line positions for the (100) sector are relatively higher values (approximately 1330 cm^{-1}). However, the values around the (111) sector are approximately 1310 cm^{-1}, which is the minimum level of the line position. The map for the full width at half-maximum of one phonon diamond line (Figure 7D) shows that the value of the line width varies from 10 to 40 cm^{-1}. The lower values of approximately 15 cm^{-1} were obtained around the (100) sector, and the regions for higher values (approximately 22 cm^{-1}) correspond to the (111) sector. By comparing the maps for the line intensity (Figure 7B), the line position (Figure 7C), and the line width (Figure 7D), the excellent correlation between the three maps can be clarified.

The line shapes and spectral features of two Raman spectra for the (100) and (111) growth sectors using Raman maps are compared. Figure 7E shows the Raman spectrum at the (100) growth sector. In this spectrum, the diamond line exhibits the highest intensity and narrower line width. The peak position is 1327 cm^{-1} and the line width is 15.6 cm^{-1}. At the (111) sector (Figure 7E), the Raman spectrum shows the lowest level of the line intensity (ca. 200 counts s^{-1}). The line position was downshifted to approximately 1312 cm^{-1}, and the line width was significantly broadened to 21.9 cm^{-1}, which are reflected by the higher level of the dopant incorporation than those for (100). As will be presented in the next section, the diamond line position is shifted to the lower wavenumber side and the line width is broadened with increasing boron doping level. It has been reported that the decrease of the intensity (the asymmetry) of the one phonon band, the downshift of the line position, and the widening of the line width are all affected by the Fano interference due to the doping of impurity. The degree of the change in the spectral feature depends on the doping levels of boron in the diamond.[19]

Therefore, it can be summarized that the heterogeneity for Raman spectra at the polycrystalline diamond surface might be mainly due to the microcrystallite-based heterogeneity for the boron doping level. Although polycrystalline diamond films were synthesized under a single B/C ratio (10^4 ppm) in the acetone−methanol−B_2O_3 solution used for the CVD synthesis, the resulting film was composed of microcrystals with different boron doping levels (semiconductor and semimetallic microcrystals). This heterogeneity for the boron doping level at the polycrystalline diamond has been suggested by the $I-V$ characteristics[22] and the transfer coefficient and rate constant for the redox reaction.[23] Additionally, for the boron-doped diamond single crystal, difference in the electrochemical behavior (the rate of electron transfer for $Fe(CN)_6^{3-/4-}$) of an individual face of single crystal due to different boron concentrations has been reported.[24] In this study, it could be clearly shown that the microscopic heterogeneity for the conductivity on the polycrystalline diamond surface stemmed from the heterogeneity for the boron doping level at individual microcrystals, resulting in the microcrystallite-based heterogeneity for the electrochemical reactivity.

The other parameters that should be analyzed for Raman spectra are the intensities of the amorphous carbon peak observed at 1500 cm^{-1} and the intensity of the background photoluminescence (PL). The intensity of the amorphous carbon peak and the PL background decreased with increasing boron doping level (see next section). For heavily boron doped sample (10^4 ppm B/C), the peak of the nondiamond sp^2 carbon inclusion and the PL background were not observed, as shown in Figure 7E,F. Therefore, the amount of the nondiamond impurity was a trace level at the heavily doped diamond film (10^4 ppm B/C). These results also indicate that the amount of the amorphous carbon impurity is closely related to the PL.

In this study, the intensity of the diamond Raman line was used as an indicator for the boron concentration in (100)- and (111)-oriented microcrystallites. However, it is better to measure the boron composition on the separate (100) and (111) growth sectors using secondary ion mass spectroscopy (SIMS) analysis. However, for SIMS measurement to obtain the accurate value of the boron composition, it is necessary to prepare the polished surface of the sample. The polishing of diamond is not so easy due to the hardness of diamond. Also, on the polished surface,

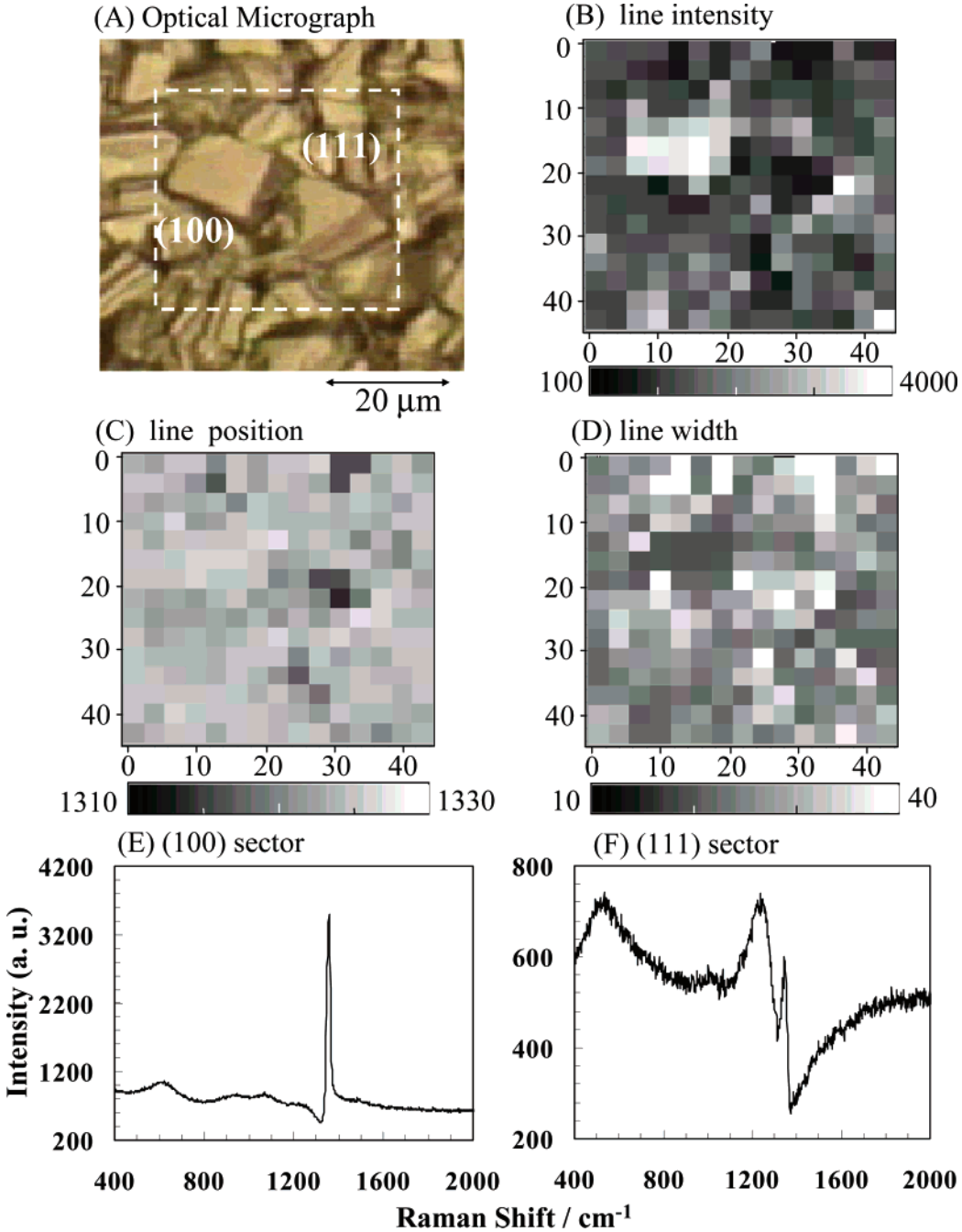

Figure 7. Optical and Raman images obtained over a 42 × 42 μm proved area at polycrystalline diamond including (100) and (111) growth sectors: (A) optical image under external illumination; (B) map for line intensity (arbitrary unit); (C) map for line position (cm^{-1}); (D) map for line width (cm^{-1}) of one phonon diamond Raman line. The diamond line frequency and width were obtained by fitting all of the individual spectra with Lorentzian line shapes. Raman spectra obtained at (E) (100) and (F) (111) growth sectors.

it is difficult to identify the location of each growth sector. Therefore, after fixing the method for identifying the location of (100) and (111) growth sectors on the polished surface, the boron composition on the separate (100) and (111) growth sectors and its dependence on the B/C ratio will be reported.

5. Dependence of the One Phonon Raman Line on the Boron Concentration. To estimate the difference in boron doping levels between the (100) and (111) growth sectors deposited at 10^4 ppm B/C, an analysis of the dependence of the intensity of diamond Raman line on the B/C ratio in methanol−acetone−B_2O_3 solution was carried out.

Polycrystalline diamond films with various boron concentrations were prepared with the atomic ratio B/C in the carbon source solution varying from 10 to 10^4 ppm. Both (100)- and (111)-oriented growth sectors whose top faces were nearly parallel to the substrate were proved by focusing the laser beam on a single microcrystallite, and Raman spectra were recorded from each type of oriented microcrystallite. The spectral changes for the (100) and (111) growth sectors are presented in Figures 8 and 9. Figure 8 shows the full-scale spectra and Figure 9 shows the magnified spectra to clearly present the lower intensity peaks. For the one phonon Raman peak observed in Figure 8, the peak positions and the values of the full widths at half-maximum are summarized in Table 1. In Figure 8, the effect of boron addition is systematically reflected in the spectral feature of the one phonon Raman peak for both (100) and (111) sectors: the downshift of Raman frequency; the broadening of the bandwidth with increasing B/C ratio; the asymmetry of one phonon band.

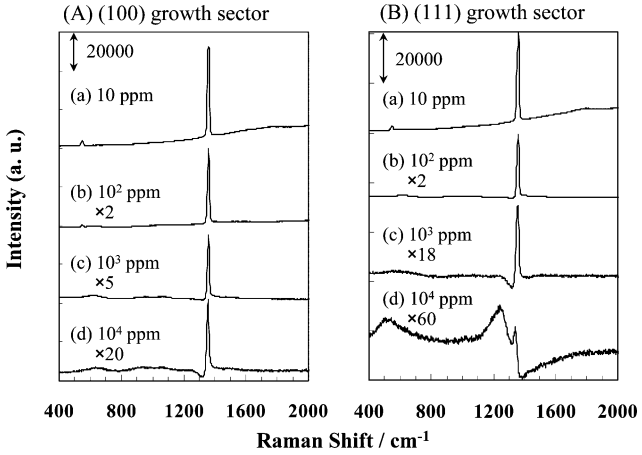

Figure 8. Raman spectra of (A) (100) and (B) (111) growth sectors for boron-doped polycrystalline diamond surface. "×2", e.g., refers to the number of magnification (2 times) of the Raman intensity.

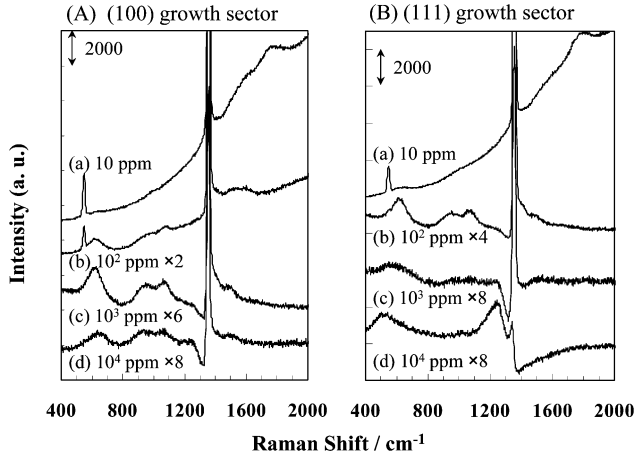

Figure 9. Magnification of Raman spectra of (A) (100) and (B) (111) growth sectors for boron-doped polycrystalline diamond surface. "×4", e.g., refers to the number of magnification (4 times) of the Raman intensity.

TABLE 1: Comparison of the Line Position and the Line Widths for the (100) and (111) Growth Sectors in Polycrystalline Diamond with Various B/C Ratios

	(100) growth sector		(111) growth sector	
B/C (ppm)	line postion (cm^{-1})	line width (cm^{-1})	line postion (cm^{-1})	line width (cm^{-1})
10	1331.8	9.4	1330.4	12.5
10^2	1330.4	12.9	1328.9	15.6
10^3	1328.9	15.7	1327.3	21.9
10^4	1327.3	21.9	1311.6	34.5

The asymmetry of the peak profile arises from the upward shift in the intensity on the high wavenumber side (Figure 9). Raman frequency progressively downshifts with increasing B/C ratio, and at B/C 10^4 ppm, values of the shift reach 4.7 and 2.4 cm^{-1} on the (100) and (111) sectors, respectively. The bandwidths increased to 21.9 cm^{-1} for (100) and 34.5 cm^{-1} for the (111) growth sector.

The bandwidth, Raman frequency shift, and asymmetry of the peak profile associated with the increase in the boron concentration have been reported to be all affected by a Fano interference.[25,26] Fano-like resonance is the interference induced by the quantum mechanical interference between the discrete phonon state and electric continuum, and such effects are well-known for Si and Ge semiconductors.[27] Similar spectral changes with increasing boron doping level in diamond have been

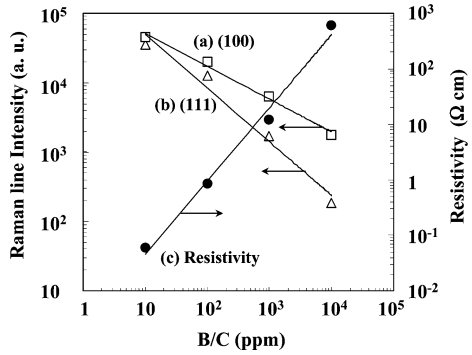

Figure 10. B/C ratio dependence of diamond Raman intensities on (a) (100) and (b) (111) growth facets and (c) resistivity of polycrystalline diamond films measured by the four-point probe method. "B/C" refers to B/C in the carbon source solution used for the CVD synthesis.

reported for homoepitaxal films, isolated microcrystals, and polycrystalline films,[19,28,29] and at higher boron concentration ($>10^{19}$ cm^{-3}), Fano-like resonance has been mentioned to be pronounced.[27]

The diamond line position is also known to be affected by local stress fluctuations caused by agglomeration of crystal grains at the polycrystalline diamond.[30] Increased Raman shift reflects compressive stress and decreased shift reflects tensile stress, and the shift due to the local stress has ranged from 1 to 5 cm^{-1}.[20] In Table 1, the values for the frequency shift at B/C 10^4 ppm (4.7 and 20.4 cm^{-1}) are relatively higher than those associated with the stress shift. Therefore, the frequency shifts at higher B/C ratios ($>10^3$ ppm) are mainly attributable to the Fano-like effect.

The decrease of the intensity of the diamond Raman line might be also affected by the transmissivity of the boron-doped diamond. The higher boron is doped in diamond, the more optically dense the material becomes. In consequence, the diamond line intensity is supposed to decrease strongly. In a series of Raman spectra (Figure 9), small peaks attributable to first-order Si Raman line were obtained at approximately 520 cm^{-1} for the (100) sector (10 and 10^2 ppm) and the (111) sector (10 ppm). Silicon wafers (Komotu Electronics Metals Co., Ltd.) were used as a substrate material on which the polycrystalline diamond was deposited (average thickness of 20 μm). Si Raman lines were not observed at higher B/C ratios than 10^3 ppm, indicating that the transmissivity of diamond decreased with increasing B/C ratio.

The resistivities of the polycrystalline diamond films used in this analysis were examined by the four-point prove method. These values are expected to reflect the average values of boron concentration in the film. The film resistivity exhibits a linear relation to the B/C ratio, as shown in Figure 10. In contrast, the intensities of the diamond Raman line at the (111)-oriented growth sector are inversely proportional to the B/C ratio, as shown in Figure 10. As a result, it was clarified that due to the combination effect of the Fano and the decrease in the transmissivity of diamond with the B/C, the diamond line intensities are inverse linearly related to the boron concentration in the diamond. Therefore, it can be expected that the boron concentration in (100)- and (111)-oriented microcrystallites can be estimated from the intensities and the features of asymmetry of one phonon diamond line.

Comparing two series of Raman spectra at each growth sector (Figure 8), the degree of intensity decreasing at the (111) sector is different from that at (100). In particular, at higher B/C ratios over 10^3 ppm, the peak intensities at the (100) facet show

relatively higher values than that at (111), and the intensity for (100) at 10^4 ppm B/C is roughly equal to that for (111) at 10^3 ppm.

Figure 10 compares the relationship between the diamond line intensities and the B/C ratio for the (100) growth sector with those for (111). The values of the line intensity were estimated by fitting the Lorentzian line shape and subtracting the background. There is not much difference in the diamond line intensities at lower doping levels (10 and 10^2 ppm) for each growth facet. However, at 10^3 ppm B/C, the intensity for the (100) facet (approximately 7000 counts s^{-1} (cps)) is approximately 5 times higher than that for (111) (approximately 1500 cps). Moreover, at the highest doping level (10^4 ppm B/C), the difference becomes increasingly prominent and the intensity for (100) (ca. 2000 cps) is approximately 10 times higher than that for the (111) facet (ca. 150 cps). In Figure 10, the intensity for the (100) facet at 10^4 ppm corresponds to that at approximately 800 ppm for (111). Supposing the inverse linear relation between the diamond line intensity and the conductivity of microcrystallites,[19,21] at 10^4 ppm B/C ratio, the conductivity for (100)-oriented microcrystallite is estimated to be only 1/12 that for (111)-oriented microcrystallite.

By way of comparison of the asymmetry and intensity of the diamond line with spectra published by Ushizawa et. al.,[19] the boron doping levels for the (111) and (100) growth sectors are estimated to be approximately 7.5×10^{20} and 5.0×10^{19} cm^{-3}, respectively. These results also suggest that the boron concentration in (100)-oriented microcrystallite was 1 order of magnitude lower than that in (111)-oriented microcrystallite.

As a result, it was summarized that, at the depositional condition of the polycrystalline diamond films used in this study (the constant B/C ratio in acetone−methanol−B_2O_3 solution), the resulting polycrystalline films contain a mixture of microcrystals with different boron doping levels (i.e., semimetallic and semiconductor). This microcrystallite-based heterogeneity for the boron doping level induces the inhomogeneity of conductivity at the polycrystalline diamond surface, resulting in the microheterogeneity for the electrochemical reactivity.

In addition, there are three other features in the series of Raman spectra (Figures 8 and 9), as described below. First, in Figure 9, at both growth sectors at 10 ppm B/C, the background signal shows a steep slope due to the photoluminescence (PL). The slope decreases with increasing B/C ratio, and the PL background could not be observed over 10^3 ppm for the (100) facet and 10^2 ppm for (111). Similar behavior has been reported for polycrystalline diamond films with boron concentration under 2×10^{19} cm^{-3}.[21] This background signal at lower boron doping levels has been explained to be caused by the luminescent defect centers that reach a minimum value at $(1-3) \times 10^{19}$ cm^{-3} boron concentration.[21] Recent work on the relationship between the luminescent signal and the broad amorphous carbon Raman signal peaking at 1500 cm^{-1} has shown that the PL arises from absorption of the excitation light by localized amorphous nondiamond inclusion.[20,31] In Figure 9, the intensities of the broad bands centered at ca. 1500 cm^{-1} assigned to disorder graphite are relatively higher at the lower B/C (<100 ppm) for the (100) and (111) sectors and the graphite band diminishes with increasing B/C ratio, indicating the close relation between the PL and the nondiamond carbon inclusion.

Three additional peaks at 610, 925, and 1045 cm^{-1} were observed at medium B/C ratios (Figure 9). The intensities of these peaks progressively increase with B/C and reach maximum values at 10^3 ppm for the (100) sector and at 10^2 ppm for (111). Boron concentrations for these microcrystallites that show the maximum intensities are estimated to be equal from the intensity of one phonon diamond line, as described previously. These weak intensity peaks have been mentioned in the literature a few times. Wang et al. have observed these peaks for the CVD-grown epitaxial layer only at the (100) facet, and not at (111).[32] These peaks have been assigned to the Raman peaks due to the breakdown of crystal momentum conservation rule. In the case of the boron incorporation into the diamond lattice, the symmetry of the crystal is broken, and the crystalline selection rule becomes are invalid; then the phonon far from the center of Brillouin zone with their momentum $q \neq 0$ can take part in Raman scattering. The peaks have been reported to be reflected by different phonon disperse properties along the (100) and (111) directions. However, in Figure 9, three peaks are observed independent of the growth sectors. Two Raman spectra at 10^4 ppm for both growth sectors are quite identical to those presented by Wang et al.[32] Therefore, it appears that these Raman signals are mainly related to the boron incorporation and are clearly observed at medium B/C ratios. The assignment for these weak Raman peaks is not identified. A possible explanation is thought to be the phonon peaks due to the breakdown of the crystal momentum selection rule and the electronic Raman scattering. To clarify the interpretation for these peaks, the dependence of scattering intensity of these bands on the excitation frequency will be examined.

At the highest B/C ratio (10^4 ppm), two broad bands centered ca. 420 and 1220 cm^{-1} appear for the (111)-oriented growth sector, as shown in Figure 9. These broad bands are well-known for heavily boron doped diamond samples.[33,34] These peaks for isolated microcrystals become pronounced at over 400 ppm B/C for the (111) growth sector and 10^3 ppm for (111), and the dependence of scattering intensities of these bands does not follow ω^4 dependence (ω is the frequency of excitation laser light).[19] Hence, these broad bands obtained in Figure 9 also might be assigned to electronic Raman scattering caused by impurity-induced electronic state.

Therefore, we can conclude that both sets of extra peaks are related to the boron incorporated in the crystal. Three additional peaks observed at moderate B/C ratios cannot be identified. By clarifying the interpretation of these peaks, detailed information about the structure of the impurity band formed near the valence band top can be obtained.

Conclusions

Electrogenerated chemiluminescence (ECL) was used to investigate the microstructure−reactivity relationship on heavily doped polycrystalline diamond surface. ECL was generated by the reaction of $[Ru(bpy)_3]^{2+}$ and tripropylamine, and images of the chemiluminescence patterns at the polycrystalline diamond surface were recorded photographically after magnification using a microscope.

In the ECL images, the square-shaped regions exhibited extremely lower ECL intensities and these regions correspond to the (100)-oriented growth sectors. This spatial distribution for ECL intensity indicates the microcrystallite-based heterogeneity for the electrochemical reactivity at the polycrystalline diamond surface.

To obtain detailed information on the structure−reactivity relationship, the variations in the ECL intensities on the lines including the (100) and (111) growth sectors and intercrystalline grain boundaries were examined. The ECL intensities on the grain surface of the (100)-oriented microcrystallite showed the lowest level of ECL reactivity. The intensities for (100) remained at approximately 50% that for (111) even at the

potential at which the average ECL intensity reached maximum (2.0 V vs Ag/AgCl), indicating that the ECL reaction rate at the (100) facets is approximately 50% of (111) at maximum. At the sites that correspond to the ridges on the (111) growth facet, ECL peaks were obtained. The peak intensities were approximately 1.2 times higher than those on the surface of (111)-oriented microcrystallite. This enhancement of ECL reactivity at these sites might be due to an effect similar to that of a microelectrode. At the ridges on the (100) growth facet, the ECL intensity was significantly enhanced (approximately 1.4−1.5 times). As the ECL reactivity on the grain surface of (100)-oriented microcrystallite was relatively low, the strong enhancement at the ridges on the (100) facet can be explained by the combination of the microelectrode effect and the increase in the amount of the reactant molecule supplied from the electrolyte phase on the (100) facet by parallel diffusion.

The ratios of the ECL intensities for the (111) growth sector to the average ECL intensity showed a constant value (approximately 1) in all potential ranges examined. In contrast, the values for the (100) growth sector linearly increased with increasing potential, indicating that the (100) growth sector required more overpotential than other regions to drive the ECL reaction. These results suggest that the conductivity at (100)-oriented microcrystallite is remarkably lower than that for (111), resulting from the microcrystallite-based heterogeneity for boron concentration.

Micro-Raman imaging was used to clarify the difference in the boron concentration between each type of oriented microcrystallite at the polycrystalline diamond. Raman spectra were collected from an area over $42 \times 42\ \mu m^2$ including the (100) and (111) growth facets at intervals of 3 μm. The map for the intensities of one phonon diamond line is also inhomogeneous over the area and shows the inverse relation with the ECL image. The regions of maximum line intensity correspond to the (100) growth sector and the values are approximately 8 times higher than those at the (111) sector.

The dependence of Raman intensity on the atomic ratio of boron to carbon (B/C) was examined. B/C was the ratio in the carbon source solution used for CVD diamond synthesis. The decrease of the line intensity of the one phonon band, the downshift of the line position, and the broadening of the line width with increasing boron concentration in diamond were obtained.

By way of comparison of the intensity of the diamond Raman line, the boron concentration for the (100) growth sector deposited at 10^4 ppm B/C was found to be the same level as that for the (111) sector at 10^3 ppm. The heterogeneity for the feature of Raman spectra at the polycrystalline diamond surface is mainly due to the microcrystallite-based heterogeneity for the boron doping level. Heavily doped polycrystalline diamond contains microcrystals with different boron doping levels, i.e., semiconductor and semimetallic diamond microcrystals.

The microstructural heterogeneity for boron concentration results in the heterogeneity for electrochemical reactivity at the heavily doped polycrystalline diamond. It has been reported that the electron-transfer rate for inorganic redox species at the polycrystalline diamond electrode depends on the variation in the functional group on the diamond surface. For example, the electron-transfer rate for the redox system with negative charge ($Fe(CN)_6^{3-/4-}$) decreased at the oxidized diamond surface due to the repulsive force from the negative surface charge density at oxygen termination.[35] At the polycrystalline diamond, a hydroxyl group can be formed on both the (111) and (100) sectors. However, a carbonyl group cannot be formed on the surface of the (111) growth sector due to the direction of the termination bonding. As the results obtained in this study suggest, the contribution of the (100) growth sector to electrochemical reactivity is relatively lower than that of other growth sectors. Therefore, the decreasing of the electron-transfer rate to redox species with negative charge at the oxidized diamond might be mainly affected by a hydroxyl group (the (111) growth sector), not by a carbonyl group (the (100) growth sector). For the comprehensive study on the electrochemical property of the polycrystalline diamond, the microcrystallite-based heterogeneity for ECL is expected to play an important role in linking the electrochemical property and the nanoscale surface structure, i.e., surface atoms and functional groups.

In electrochemical application of boron-doped diamond, higher reactivity is necessary. To achieve higher electrochemical reactivity, the polycrystalline diamond should be composed of microcrystals with higher conductivity. From the results in this study, polycrystalline films without the (100) growth sector are expected to have the advantage as an electrode material for electrochemical applications. In microwave-assisted CVD synthesis for the polycrystalline diamond, it has been reported that the distribution of growth sectors could be controlled by selecting the substrate temperature and CH_4 concentration during the deposition, and that the texture of the resulting film was mainly (111)-oriented microcrystallites at low substrate temperature.[36] To develop the ECL detector with higher sensitivity (higher ECL intensity), the synthesis of the polycrystalline film without the (100) growth sector should be attempted and the optimization of the performance of the ECL detector will be carried out.

References and Notes

(1) Martin, H. B.; Argoitia, A.; Landau, U.; Anderson, A. B.; Angus, J. C. *J. Electrochem. Soc.* **1996**, *143*, L133.
(2) Swain, G. M.; Anderson, A. B.; Angus, J. C. *MRS Bull.* **1998**, *23*, 56.
(3) Swain, G. M. *J. Electrochem. Soc.* **1994**, *141*, 3382.
(4) Rao, T. N.; Fujishima, A. *J. Diamond Relat. Mater.* **2000**, *9*, 3.
(5) Granger, M. C.; Swain, G. M. *J. Electrochem. Soc.* **1999**, *146*, 12.
(6) Popa, E.; Notsu, H.; Miwa, T.; Tryk, D. A.; Fujishima, A. *Electrochem. Solid-State Lett.* **1999**, *2*, 49.
(7) Olivia, H.; Sarada, B. V.; Honda, K.; Fujishima, A. *Electrochim. Acta* **2004**, *49*, 2069.
(8) Ivandini, T. A.; Sarada, B. V.; Terashima, C.; Rao, T. N.; Tryk, D. A.; Ishiguro, H.; Kubota, Y.; Fujishima, A. *J. Chromatogr., B* **2003**, *791*, 63.
(9) Terashima, C.; Rao, Tata, N.; Sarada, B. V.; Tryk, D. A.; Fujishima, A. *Anal. Chem.* **2002**, *74*, 895.
(10) Uchikado, R.; Rao, Tata, N.; Tryk, D. A.; Fujishima, A. *Chem. Lett.* **2001**, 144.
(11) Honda, K.; Yoshimura, M.; Rao, Tata, N.; Fujishima, A. *J. Phys. Chem. B* **2003**, *107*, 1653.
(12) Zu, Y.; Bard, A. J. *Anal. Chem.* **2000**, *72*, 3223.
(13) Wang, J.; Swain, G. M.; Mermoux, M.; Lucazeau, G.; Zak, J.; Strojek, J. W. *New Diamond Frontier Carbon Technol.* **1999**, *9*, 317.
(14) Spitsyn, B. V.; Bouilov, L. L.; Deryagin, B. V. *J. Cryst. Growth* **1981**, *52*, 219.
(15) Janssen, G.; van Enckevort, W. J. P.; Vollenberg, W.; Giling, L. J. *Diamond Relat. Mater.* **1990**, *1*, 789.
(16) Angus, J. C.; Martin, H. B.; Landau, U.; Evstefeeva, Y. E.; Miller, B.; Vinokur, N. *New Diamond Frontier Carbon Technol.* **1999**, *9*, 175.
(17) Yano, T.; Tryk, D. A.; Hashimoto, K.; Fujishima, A. *J. Electrochem. Soc.* **1998**, *145*, 1870.
(18) Notsu, N.; Yagi, I.; Tatsuma, T.; Tryk, D. A.; Fujishima, A. *J. Electroanal. Chem.* **2000**, *429*, 31.
(19) Ushizawa, K.; Watanabe, K.; Ando, T.; Sakaguchi, I.; Nishitani-Gamo, M.; Sato, Y.; Kanda, H. *Diamond Relat. Mater.* **1998**, *7*, 1719.
(20) Mermoux, M.; Marcus, B.; Swain, G. M.; Butler, J. E. *J. Phys. Chem. B* **2002**, *106*, 10816.
(21) Colineau, E.; Gheeraert, E.; Deneuville, A.; Mambou, J.; Brunet, F.; Lagrange, J. P. *Diamond Relat. Mater.* **1997**, *6*, 778.
(22) Vinokur, N.; Miller, B.; Avyigal, Y.; Kalish, R. *Electrochem. Solid-State Lett.* **1998**, *1*, 265.

(23) Modestov, A. D.; Evstefeeva, Yu. E.; Pleskov, Yu. V.; Mazin, V. M.; Varnin, V. P.; Terametskaya, I. G. *J. Electroanal. Chem.* **1997**, *431*, 211.

(24) Pleskov, Yu. V.; Evstefeeva, Yu. E.; Krotova, M. D.; Mishuk, V. Ya.; Laptev, V. A.; Palyanov, Yu. N.; Borzdov, Yu. M. *J. Electrochem. Soc.* **2002**, *149*, E260.

(25) Fano, U. *Phys. Rev.* **1961**, *124*, 1866.

(26) Cerdeira, F.; Fjeldly, T. A.; Cardona, M. *Phys. Rev. B* **1973**, *8*, 4734.

(27) Abstreiter, G.; Cardona, M.; Pinczuck, G. In *Light Scattering in Solid*; Cardona, M., Guntherodt, G., Eds.; Topics in Applied Physics 54; Springer-Verlag: Berlin, 1984; p 5.

(28) Pruvost, F.; Deneuville, A. *Diamond Relat. Mater.* **2001**, *10*, 531.

(29) Ager, J. W., III; Walukiewicz, W.; McCluskey, M.; Plano, M. A.; Landstrass, M. I. *Appl. Phys. Lett.* **1995**, *66*, 616.

(30) Gheeraert, E.; Deneuville, A.; Bonnot, A. M.; Abello, L. *Diamond Relat. Mater.* **1992**, *1*, 525.

(31) Xu, J.; Granger, M. C.; Chan, Q.; Strojk, J. W.; Lister, T. E.; Swain, G. M. *Anal. Chem. News Future* **1997**, 591A.

(32) Wang, Y.; Li, H.; Lin, Z.; Feng, K. *Jpn. J. Appl. Phys.* **2000**, *39*, 2795.

(33) Gonon, P.; Gheeraert, E.: Deneuville, A.; Fontaine, F.; Abello, L.; Lucazeau, G. *J. Appl. Phys.* **1995**, *78*, 7059.

(34) Zhang, R. J.; Lee, S. T.; Lam, Y. W. *Diamond Relat. Mater.* **1996**, *5*, 1288.

(35) Yagi, I.; Notsu, H.; Kondo, T.; Tryk, D. A.; Fujshima, A. *J. Electroanal. Chem.* **1999**, *473*, 173.

(36) Ando, Y.; Tachibana, T.; Kobashi, K. *Diamond Relat. Mater.* **2001**, *10*, 312.